Thermochimica Acta, 174 (1991) 201–221
Elsevier Science Publishers B.V., Amsterdam

THERMAL BEHAVIOR OF THE CHEVREL PHASE SULFIDES

TAKASHI UCHIDA and MASATAKA WAKIHARA

Department of Chemical Engineering, Tokyo Institute of Technology, Meguro-ku, Tokyo 152 (Japan)

(Received 9 October 1989)

ABSTRACT

The Chevrel phase sulfides $M_xMo_6S_{8-y}$ (M ≡ metal) have attracted attention because of their high superconducting critical temperatures and high critical fields. However, much less attention has been paid to their thermal and/or thermochemical properties. In this review, thermochemical features of the Chevrel phase sulfides, such as phase relations of $M_xMo_6S_{8-y}$, thermochemical properties and thermal stability in air, are discussed.

INTRODUCTION

The ternary molybdenum sulfides having the formula $M_xMo_6S_8$ (M ≡ metal), the so-called Chevrel phase sulfides, have been studied intensively since the discovery of their unique crystal structure [1] and interesting low temperature physical properties, i.e., high superconducting transition temperatures ($PbMo_6S_8$: $T_c \approx 15$ K [2]) and very high critical fields ($PbMo_6S_8$: $H_{c2} \approx 60$ T [3]). Recently these compounds have attracted attention also because of their potential application as cathode material for high energy density lithium secondary batteries [4–6]. As described in the review article by Yvon [7] on the crystal structure and physical properties of the Chevrel phase compounds, the crystal structure of the Chevrel phase sulfides is characterized by a three-dimensional stacking of nearly cubic Mo_6S_8 clusters, each of which is made up of eight chalcogen atoms located at the corners of the cube and six molybdenum atoms nearly at its six face centers. Many of the Chevrel phase sulfides crystallize in a hexagonal–rhombohedral structure at room temperature. (Some of them, such as $Cr_2Mo_6S_8$, exhibit a triclinic structure which is a distorted form of the rhombohedral structure [1]. At lower temperatures, some of the rhombohedral phases transform into the triclinic structure [8], as will be described later.) The crystal structures of the Chevrel phase sulfides, together with hexagonal and rhombohedral unit cells and the rhombohedral $\bar{3}$ axis, are illustrated in Figs. 1 and 2a. A second metal element, M, occupies a site inbetween two Mo_6S_8 clusters neighboring

0040-6031/91/$03.50

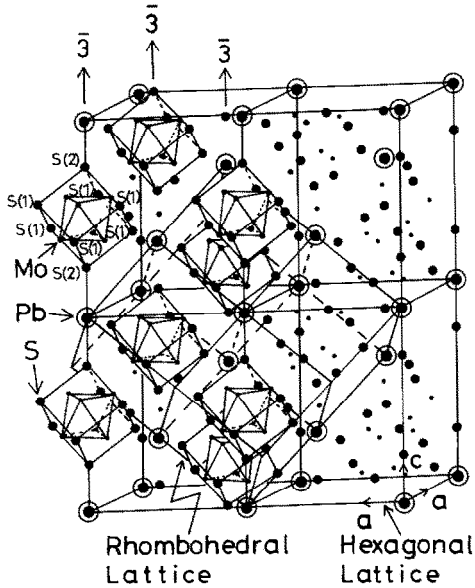

Fig. 1. Crystal structure of $Pb_xMo_6S_8$ on the basis of the data given in ref. 7.

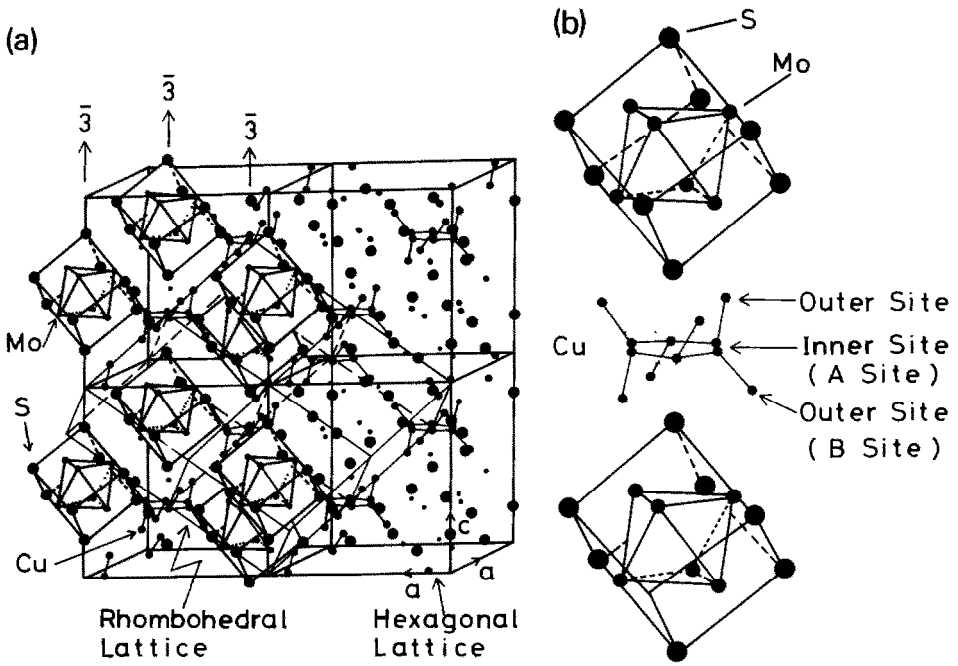

Fig. 2. a, Crystal structure of $Cu_xMo_6S_8$ using ref. 7; b, two sets of sixfold copper sites of $Cu_xMo_6S_{8-y}$.

along the $\bar{3}$ axis. When M is a large cation such as Pb^{2+}, Sn^{2+} or Ag^{+}, the composition of M (the x value in the formula $M_xMo_6S_8$) is nearly 1 and M is localized on the origin of the rhombohedral unit cell. When, however, the M cation is small, such as Cu^{+}, Ni^{2+} or Fe^{2+}, the values of x are usually larger than 1 and the cations are randomly distributed in the 12 metal sites which are away from the $\bar{3}$ axis, as shown in Fig. 2a. These 12 sites are made up of two sets of six-fold sites which are called inner tetrahedral sites (A sites) and outer tetrahedral sites (B sites), as illustrated in Fig. 2b. In general, compounds containing large cations have a rhombohedral cell angle $\alpha_R \approx 89°–91°$ ($PbMo_6S_8$: $\alpha_R = 89.27°$), while those containing small cations have values $\alpha_R \approx 94°–95°$ [7]. The Chevrel phase sulfides can thus incorporate different concentrations of a variety of metal elements having a range of size, atomic number, and ionic potential. The Chevrel phase compounds are usually stable in a chalcogen deficient form [7,9,10]. Accordingly, the general formula of the Chevrel phase compounds is expressed as $M_xMo_6S_{8-y}$ in this article.

Since the most striking features of this material are the unusual physical properties at low temperatures, including high superconducting transition temperatures and high critical fields, there have been a great many investigations and also several reviews on this subject [7,11,12]. However, only little is known about the phase relations and/or thermal behavior of the Chevrel phase sulfides.

In this article, the phase relations of the ternary Chevrel phase sulfides are reviewed in the first section, while the second section deals with thermodynamics and thermal effects. In the final section, stability of the Chevrel phase sulfides in air at elevated temperatures is described.

PHASE RELATIONS

In Fig. 3, the metal elements which can be incorporated into the Chevrel phase sulfides are summarized in the form of a periodic table after Fischer [11] with some modification. The "r" and "t" in this figure represent the rhombohedral and triclinic structures at room temperature, respectively. "r, t" means that the phase crystallizes in both the rhombohedral and triclinic structures depending on its composition, e.g., $Fe_xMo_6S_8$ [13]. In Fig. 3, the M elements which form compounds with $\alpha_R > 94°$ when the M cation is small are shaded.

Copper Chevrel-phase sulfides ($Cu_xMo_6S_{8-y}$)

Copper is a small cation, and the copper Chevrel phase sulfides exhibit a rather wide range of nonstoichiometry. Flükiger et al. [14] have reported the temperature dependence of the solubility limit of copper (x in $Cu_xMo_6S_{8-y}$),

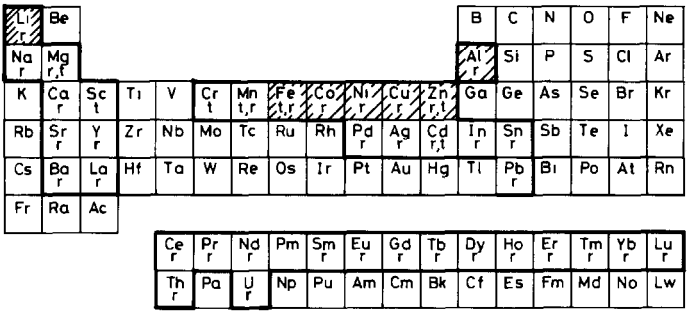

Fig. 3. Periodic table indicating the M elements which form Chevrel phase sulfides. The room temperature phase is rhombohedral (r) or triclinic (t). Chevrel phase sulfides having shaded elements have α_R values greater than 94°. From ref. 11 with some modifications.

at temperatures from 850 °C to 1750 °C (Fig. 4). Flükiger et al. first melted the sample in an induction furnace using an Al_2O_3 crucible at argon pressures between 20 atm and 100 atm, followed by homogeneization for 1 h at 1500 °C, and then quenching. In order to obtain precise information about the phase limits, the samples were annealed in quartz ampoules at temperatures from 850 °C to 1450 °C. It may be seen in Fig. 4 that the rhombohedral $Cu_xMo_6S_8$ phase is formed congruently from the melt at 1750 ± 30 °C, and that the rhombohedral phase exhibits a rather wide

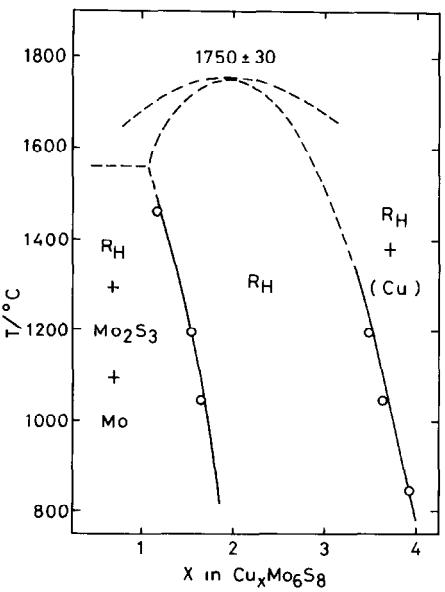

Fig. 4. The high temperature phase diagram of the system $Cu_xMo_6S_8$, redrawn from ref. 14. R_H represents the rhombohedral Chevrel phase.

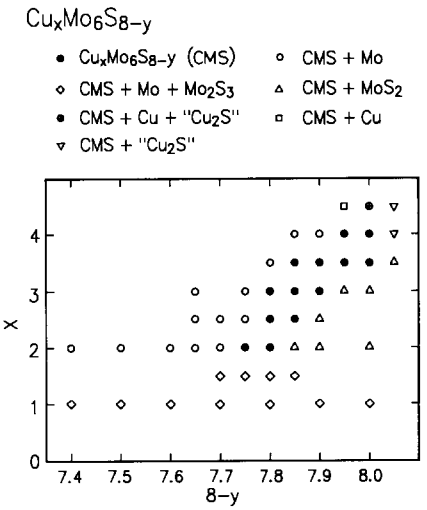

Fig. 5. The single phase region and the phase relations of the copper Chevrel phase sulfides $Cu_xMo_6S_{8-y}$ at 1000 °C, from ref. 15.

homogeneity range. Furthermore, the phase limits are strongly temperature dependent, i.e., $1.2 \leqslant x \leqslant 3$ at 1500 °C while $1.8 \leqslant x \leqslant 4$ at 850 °C. However, Flükiger et al. have estimated the sulfur composition only roughly from the lattice parameters. As described earlier, the Chevrel phase sulfides usually have a sulfur deficiency, and the phase limits with respect to the copper content, x, should be influenced by the sulfur content, $8-y$, in $Cu_xMo_6S_{8-y}$. The sulfur nonstoichiometry of the copper Chevrel phase sulfides has studied by Cheung and Steele [10]. They prepared samples by direct combination of the elements at 1100 °C in evacuated quartz ampoules. This preparation technique for the Chevrel phase sulfides has been used by most of the researchers cited in this article and hereafter the preparation procedure will not be mentioned if the sample was prepared in this manner. Cheung and Steele have shown that the nonstoichiometry range of sulfur, $8-y$, in $Cu_2Mo_6S_{8-y}$ (compound with $x=2$) was $7.7 \leqslant 8-y \leqslant 7.85$. In our research group we have prepared copper Chevrel phase sulfides having various compositions with respect to both x and $8-y$ at 1000 °C, and have determined the homogeneity range of $Cu_xMo_6S_{8-y}$ [15] using X-ray diffractometry (Fig. 5). A stoichiometric composition, $Cu_4Mo_6S_{8.0}$, was obtained in this system. Figure 5 shows that the nonstoichiometry range with respect to x at a certain sulfur content is not as large as that shown in Fig. 4: for example, at $(8-y)=7.8$, $2 \leqslant x \leqslant 3$; at $(8-y)=7.9$, $3 \leqslant x \leqslant 3.5$; and at $(8-y)=8.0$, $3.5 \leqslant x \leqslant 4$. Accordingly, the sulfur contents of the samples in the copper rich end ($x \approx 4$) and in the copper poor end ($x \approx 2$) in Fig. 4 should be different.

Figure 6 shows the phase diagram of the Cu–Mo–S system at 1000 °C.

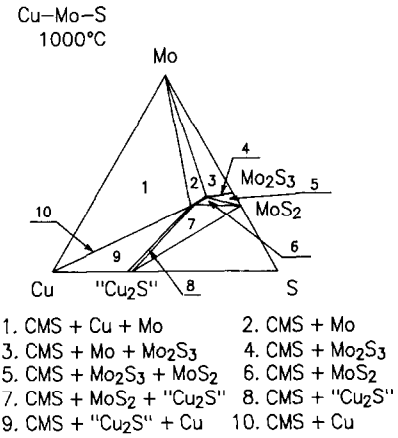

Fig. 6. The phase diagram of the Cu–Mo–S system at 1000 °C [15].

This was drawn on the basis of the equilibrium data in Fig. 5 and some additional data [15].

The variation in the rhombohedral lattice parameters for $Cu_xMo_6S_{8-y}$ with respect to x and $8-y$ [15] is shown in Fig. 7. The lattice parameters are more dependent on the copper content than on the sulfur content: however, it seems that the a_R value decreases slightly with increasing $8-y$ when the copper contents are the same.

The copper Chevrel phase sulfides having a copper content x of less than 1.8 are unstable at high temperatures, as shown in Fig. 4. They can, however, be prepared at room temperature by an electrochemical technique [13,16]

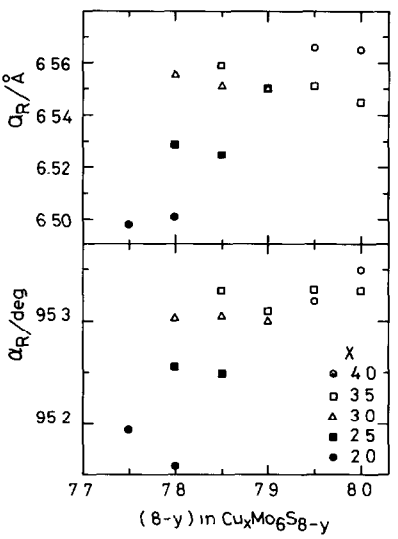

Fig. 7. Compositional variation of the rhombohedral lattice parameters of $Cu_xMo_6S_8$ [15].

starting from single phase $Cu_xMo_6S_{8-y}$ ($x > 1.8$), or by leaching methods using hydrochloric acid [17] or iodine in acetonitrile [18].

The lattice parameters of Mo_6S_{8-y} prepared in this way are $a_R = 6.432$ Å and $\alpha_R = 91.34°$ [17]. It should be noted that the α_R value drastically decreases from that of the original copper Chevrel phase, for example for $Cu_2Mo_6S_{7.8}$ $a_R = 6.501$ Å and $\alpha_R = 95.16°$. These rhombohedral lattice parameters can be converted to hexagonal parameters as follows: for $Cu_2Mo_6S_8$ $a_H = 9.598$ Å and $c_H = 10.197$ Å; and for Mo_6S_8 $a_H = 9.20$ Å and $c_H = 10.88$ Å. The following conversion equations were used for this purpose.

Hexagonal to rhombohedral

$$a_R = \left(\tfrac{1}{3} a_H^2 + \tfrac{1}{9} c_H^2\right)^{1/2} \quad (1)$$

$$\cos \alpha_R = \left(-\tfrac{1}{6} a_H^2 + \tfrac{1}{9} c_H^2\right)/a_R^2 \quad (2)$$

Rhombohedral to hexagonal

$$a_H = \left[2(1 - \cos \alpha_R)\right]^{1/2} a_R \quad (3)$$

$$c_H = \left[3(1 + 2 \cos \alpha_R)\right]^{1/2} a_R \quad (4)$$

where the subscripts R and H represent rhombohedral and hexagonal, respectively. The above comparison shows that the c parameter of Mo_6S_8 is greatly increased. This means that the copper ions in $Cu_xMo_6S_{8-y}$ strongly attract the Mo_6S_8 clusters neighboring along the $\bar{3}$ axis (see Fig. 2a).

Lead Chevrel phase sulfides ($Pb_xMo_6S_{8-y}$)

The phase relations of the lead Chevrel phase sulfides, $Pb_xMo_6S_{8-y}$ have been most intensively investigated, since among Chevrel phase compounds these compounds exhibit the highest superconducting transition temperature T_c [9]. The lead cation belongs to the group of large cations, and the composition x of lead is almost unity. However, slight non-stoichiometry with respect to x and sulfur deficiency are known.

Single phase regions with respect to both lead and sulfur contents have been reported by Krabbes and Oppermann [12,19], Hauck [20], Yamamoto et al. [21] and Yamasaki and Kimura [22]. The results given in refs. 12, 21 and 22 are summarized in Fig. 8 together with the coexisting phases shown in ref. 21. The single phase region reported by Hauck [20] ($0.85 < x < 1.05$, $6.8 < 8 - y < 7.4$ at 1000 °C) was considerably different from the other three, and is not plotted. The stoichiometric composition $PbMo_6S_{8.0}$ has not been obtained as a single phase. The single phase region determined by our research group (Yamamoto et al. [21]) shows that the homogeneous region

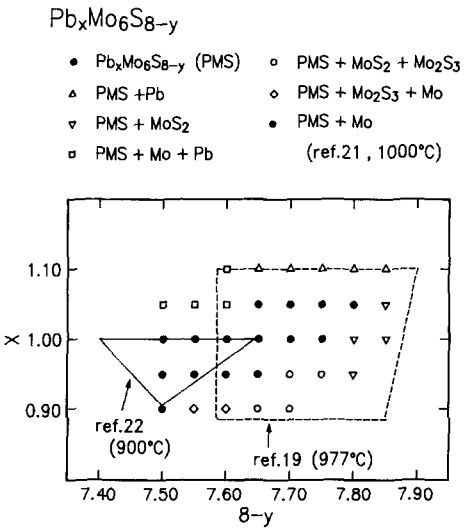

Fig. 8. The single phase regions of $Pb_xMo_6S_8$ reported in the literature.

shifts in the sulfur rich direction with increasing lead content x, similarly as observed for the copper Chevrel phase (Fig. 5).

Since no other phase besides $Pb_xMo_6S_{8-y}$ exists in the ternary Pb–Mo–S system, the phase diagram of this system was found to be very simple (Fig. 9) [21].

The rhombohedral lattice parameters reported in the literature [20–22] are plotted against x in Fig. 10. No obvious trend in the compositional variation is observed.

From DTA measurements, Hauck [20] has found that $Pb_xMo_6S_{8-y}$ decomposes peritectically at 1530 °C with a liquidus temperature of about 1600 °C. Flükiger et al. [23] also have reported that $PbMo_{6.2}S_8$, $SnMo_{6+y}S_8$

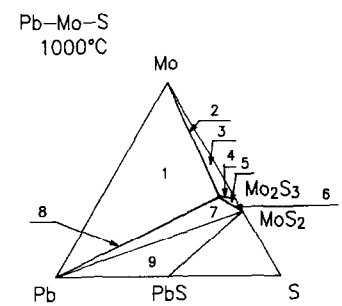

1. PMS + Pb + Mo
2. PMS + Mo
3. PMS + Mo + Mo_2S_3
4. PMS + Mo_2S_3
5. PMS + Mo_2S_3 + MoS_2
6. PMS + MoS_2
7. PMS + MoS_2 + Pb
8. PMS + Pb
9. Pb + PbS + MoS_2

Fig. 9. The phase diagram of the Pb–Mo–S system at 1000 °C [21].

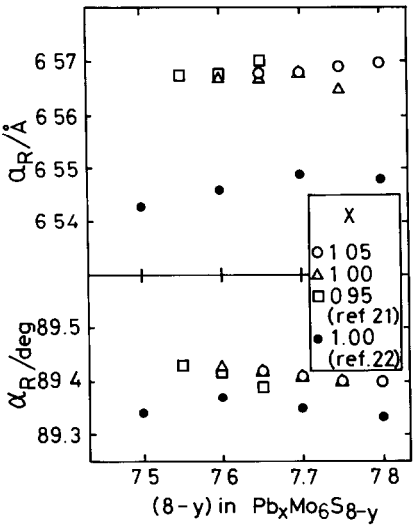

Fig. 10. Compositional variations of rhombohedral lattice parameters for $Pb_xMo_6S_8$.

and $AgMo_6S_8$ form peritectically from the melt instead of forming congruently like many other Chevrel phase sulfides, e.g. $Cu_xMo_6S_8$ (Fig. 4), $Ni_xMo_6S_8$, etc.

Iron Chevrel phase sulfides ($Fe_xMo_6S_{8-y}$)

The phase relations of the Fe–Mo–S system are rather complicated because of the existence of two additional ternary phases (monoclinic $FeMo_2S_4$ and triclinic $FeMo_3S_4$) besides the iron Chevrel phase $Fe_xMo_6S_8$ [11]. The precise phase relations of the Fe–Mo–S system at 1000 °C have been reported by Wada et al. [13] and are given in Fig. 11. Although a wide single phase region of $Fe_xMo_6S_{8-y}$ was expected because Fe^{2+} is a small cation, the observed range was small. Figure 11 shows that the rhombohedral $Fe_xMo_6S_{8-y}$ phase coexists with the triclinic $FeMo_3S_4$ phase. However, one must remember that this phase diagram is for samples quenched from 1000 °C, because the phase analysis was by means of X-ray diffraction carried out at ambient temperatures. According to Yvon et al. [24], triclinic $FeMo_3S_4$ transforms into the rhombohedral modification above 200 °C owing to an order–disorder transition of the iron atoms. Accordingly, Wada et al. have suggested that a solid solution of the rhombohedral phase in the range $Fe_xMo_6S_{8-y}$–$FeMo_3S_4$ is formed at 1000 °C because both end members have the same structure. In other words, a rather wide homogeneous range of rhombohedral $Fe_xMo_6S_{8-y}$ ($1.1 \leqslant x \leqslant 2.1$, $7.67 \leqslant 8-y \leqslant 8.12$) would exist at 1000 °C.

In Fig. 12 the compositional variations of the rhombohedral lattice parameters presented by Wada et al. are plotted only for the single phase

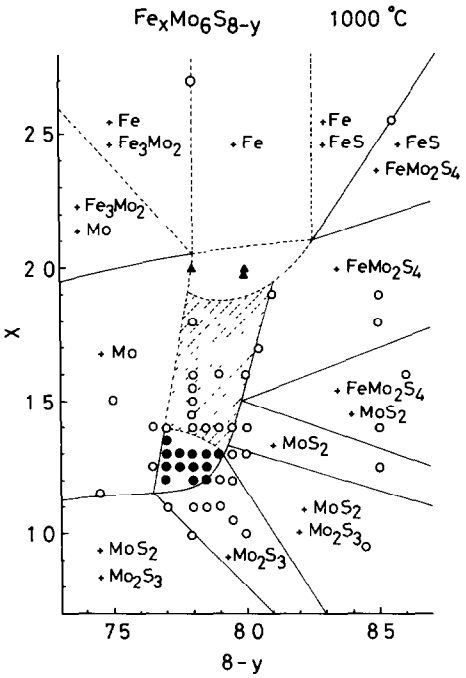

Fig. 11. The single phase region and phase relations of $Fe_xMo_6S_{8-y}$ at 1000 °C. ▲, $FeMo_3S_4$; ●, $Fe_xMo_6S_{8-y}$; - - - - - -, tie lines between $Fe_xMo_6S_{8-y}$ and $FeMo_3S_4$. Redrawn from ref. 13.

region. As in the case of the copper Chevrel phase sulfide, a_R increased with increasing iron content x. Also, a_R obviously increases with increasing sulfur content $8-y$ in this case.

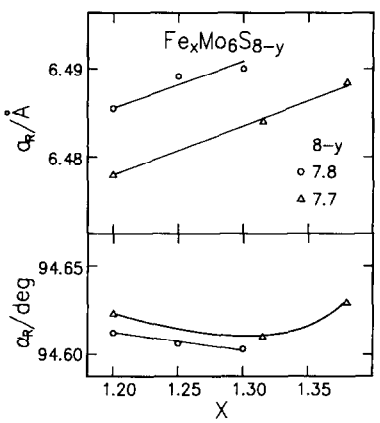

Fig. 12. Compositional variation of the rhombohedral lattice parameters in the single phase regions of $Fe_xMo_6S_{8-y}$, from Wada et al. [13].

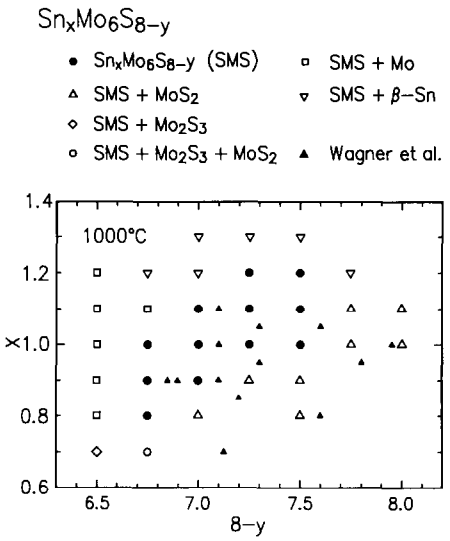

Fig. 13. The single phase region and the phase relations of the $Sn_xMo_6S_{8-y}$ reported in ref. 26. The single phase region shown in ref. 25 is also plotted. Both results were obtained at 1000 °C.

Tin Chevrel phase sulfide ($Sn_xMo_6S_8$)

The single phase region of tin Chevrel phase sulfides $Sn_xMo_6S_{8-y}$ has been reported by Wagner et al. [25] and Sato et al. [26]. In Fig. 13, the results given in the above papers are summarized. The coexisting phases reported by Sato et al. are also given. Since the tin cation is a large cation, the tin content x is around unity. It ranges, however, over a larger region ($0.70 \leqslant x \leqslant 1.2$) than that for the lead Chevrel phase (Fig. 8). Furthermore, the nonstoichiometric range of sulfur $8-y$ ($6.75 \leqslant 8-y \leqslant 7.95$) is larger than for any other system described so far in this article.

On the other hand, the compositional variation of the rhombohedral lattice parameters is fairly small, as shown in Fig. 14 (Sato et al. [26]), in spite of the wide homogeneous range with respect to both tin and sulfur contents.

Nickel Chevrel phase sulfides ($Ni_xMo_6S_{8-y}$)

The single phase region for nickel Chevrel phase sulfides $Ni_xMo_6S_{8-y}$ has been investigated by Tanjo et al. [27], and is shown in Fig. 15. Owing to the high vapor pressure at 1000 °C of the nickel sulfides, which would coexist with the Chevrel phase at high x values, ambiguity still remains concerning the phase limit in the high x region ($x \approx 2$).

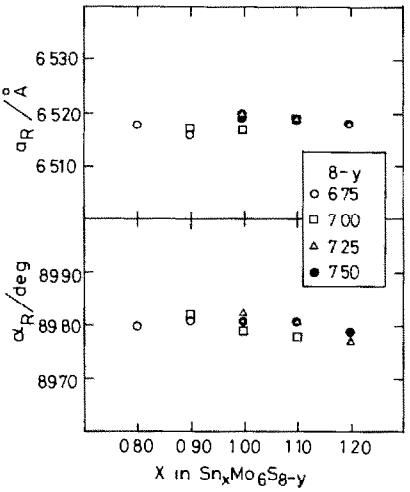

Fig. 14. Compositional dependence of the rhombohedral lattice parameters for $Sn_xMo_6S_{8-y}$ [26].

The nonstoichiometry with respect to nickel content x is rather narrow when compared with those of other Chevrel phase sulfides having small cations, e.g. $Cu_xMo_6S_{8-y}$, $2 \approx x \approx 4$; $Fe_xMo_6S_{8-y}$, $1.25 \approx x \approx 2$ (assuming that the triclinic $FeMo_3S_4$ phase transforms into the rhombohedral phase and forms a solid solution with the $Fe_xMo_6S_{8-y}$ phase at high temperatures).

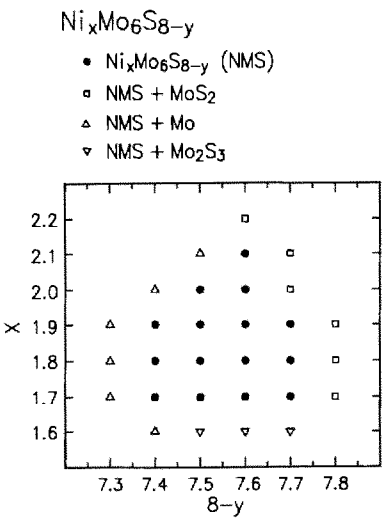

Fig. 15. The single phase region of $Ni_xMo_6S_{8-y}$ [27].

The rhombohedral lattice parameters were in the range 6.449–6.460 Å for a_R and 94.66°–94.75° for α_R [27].

Cobalt Chevrel phase sulfide ($Co_xMo_6S_{8-y}$)

Yamaguchi et al. [28] have investigated the single phase region of cobalt Chevrel phase sulfides $Co_xMo_6S_{8-y}$. It was found to be very narrow, which is limited within the range of $1.55 < x < 1.65$ and $7.65 < 8 - y < 7.75$. This phase was found to coexist with another ternary phase, $CoMo_2S_4$, in the sulfur rich side of the single phase. The rhombohedral lattice parameters were $a_R = 6.469$ Å and $\alpha_R = 95.29°$. Also, Guillevic et al. [29] have reported the composition of $Co_{0.80}Mo_{3.20}S_4$ ($Co_{1.5}Mo_6S_{7.5}$: $a_R = 6.483$ Å, $\alpha_R = 95.28°$).

Other than those described above, investigations of the single phase region for the Chevrel phase sulfides are, as far as we know, quite few in number.

Yvon [7] has previously offered an ionic–covalent bonding model of the Chevrel phase compounds, which includes the concept of cluster valence-electron-concentration (cluster VEC [7]). According to this model a maximum of four electrons can be transferred to a Mo_6S_8 cluster by incorporating M cations. This theory clearly can explain the maximum number of M cations which can be incorporated in the Chevrel phase sulfides, e.g. four Cu^+ in $Cu_xMo_6S_{8-y}$, two Fe^{2+} in $Fe_xMo_6S_{8-y}$ and two Ni^{2+} in $Ni_xMo_6S_{8-y}$, etc.

As described above, most of the Chevrel phase sulfides exhibit smaller sulfur : molybdenum ratio than 4 : 3. Accordingly, the compositions of these compounds have been expressed as $M_xMo_6S_{8-y}$ in this article. However, various models for the defect structure of the Chevrel phase sulfides have been proposed in the literature. Flükiger et al. [23] have reported that the predominant defect species in the lead Chevrel phase $PbMo_{6.2}S_8$ should be excess molybdenum atoms instead of sulfur vacancies, based on a comparison of the calculated (from X-ray data) and the measured densities. Sergent et al. [30] have also supported this model. However, Marezio et al. [31] have found, based on X-ray diffractometry of a lead Chevrel phase sulfide, that 8% of the Pb sites and 25% of the S(2) sites, which are on the $\bar{3}$ axis (see Fig. 1), are unoccupied resulting in the composition $Pb_{0.25}Mo_6S_{7.5}$. This result suggests that the predominant defect type is sulfur vacancies. Wada et al. [13] have also suggested a sulfur vacancy model for the iron Chevrel phase sulfides from density measurements. On the other hand, Yamasaki et al. [32] have concluded that both sulfur vacancies and excess Mo atoms would exist in $PbMo_6S_{8-y}$ having intermediate or large y values. More intensive investigations would be necessary for a better understanding of the defect structure of the Chevrel phase compounds.

THERMOCHEMICAL PROPERTIES AND THERMAL BEHAVIORS OF THE CHEVREL PHASE SULFIDES

Only limited information about the thermochemical properties has been reported so far, in contrast to a great many papers on physical properties.

Only one paper has been presented on the high temperature thermodynamics of the Chevrel phase compounds, by Hauck and Heiderich [33]. They have prepared lead and copper Chevrel phase sulfides from the elements under hydrothermal conditions in an autoclave, and have found that the ternary phases $PbMo_6S_8$ and $Cu_2Mo_6S_8$ (they assumed stoichiometric composition) form only above the temperatures 713 °C and 590 °C respectively. They referred to these temperatures as the decomposition temperatures. This decomposition temperature of $Cu_2Mo_6S_8$ is very close to that of $CuMo_2S_3$ (supposed to be identical with the copper Chevrel phase) reported by Grover and Moh [34], which is $594 \pm 4\,°C < T < 610 \pm 5\,°C$ (where T stands for the decomposition temperature).

Using a linear interpolation of the thermodynamic data [35] within the temperature range 700–1100 K, Grover and Moh also estimated the Gibbs energies of formation of $PbMo_6S_8$ and $Cu_2Mo_6S_8$. A part of the Gibbs energy diagram given by Hauck and Heiderich is shown in Fig. 16 in accordance with eqns. (1) and (4) in the figure. From Fig. 16, the Gibbs energy of $Cu_2Mo_6S_8$ at 1000 K is estimated to be -873 kJ mol^{-1}. Assuming that the activities of the solid Cu, Mo and $Cu_2Mo_6S_8$ are unity, the equilibrium partial pressure of sulfur from eqn (5) in Fig. 16 is calculated to

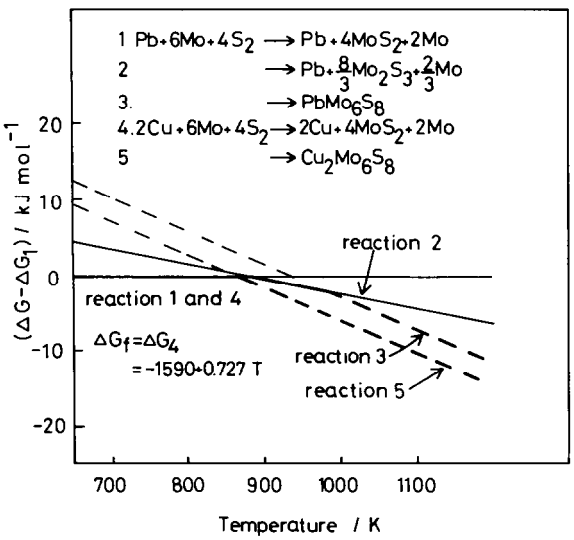

Fig. 16. The Gibbs energy diagram for the reactions (1)–(5) shown in the figure, relative to reactions (1) and (4) in the figure. Redrawn from ref. 33.

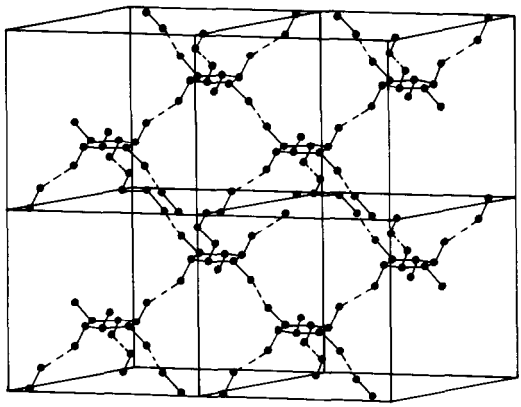

Fig. 17. Illustration of the three dimensionally interconnected copper sites in the crystal lattice of $Cu_xMo_6S_{8-y}$. Positions are calculated from ref. 7.

be log $P_{S_2} \approx -6.4$ at 1000 K, where P_{s_2} is in Pa. However, Fig. 5 shows that $Cu_2Mo_6S_{7.8}$ coexists with MoS_2. It can be estimated from the paper of Suzuki et al. [35] that MoS_2 is stable under a partial pressure of log $P_{S_2} \geqslant -5.4$ at 1000 K. Accordingly, $Cu_2Mo_6S_{8-y}$ would be stable at least in the range $-6.4 \leqslant \log P_{S_2} \leqslant -5.4$ at 1000 K.

Since copper ions can migrate through three dimensionary interconnected cation sites (Fig. 17) even at room temperature, the copper Chevrel phase sulfide is a good copper ion conductor, as well as a metallic electronic conductor [36]. Dudley et al. [36,37] have measured the copper ion conductivity of $Cu_xMo_6S_{7.59}$ at temperatures between 396 K and 441 K using a solid electrolyte in both ends of the sample. The activation energy for ionic conduction in the region $x < 2$ where copper ions mainly occupy A sites (inner sites, see Fig. 2b) [38], was higher (31 kJ mol^{-1}) than that obtained in the region $x > 2.4$ (18 kJ mol^{-1}), where occupation of B sites (outer sites) by copper ions becomes predominant [38]. They have deduced the energy profile along the Cu ion conduction path as shown in Fig. 18, and estimated

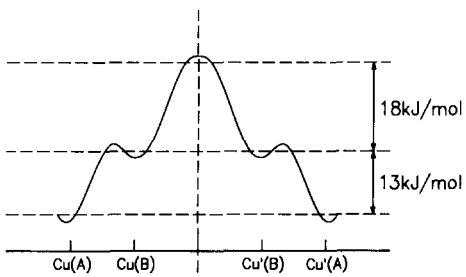

Fig. 18. Possible energy profile along the Cu ion conduction path, from ref. 37. Cu(A) and Cu(B) represent the copper cation in the A and B sites, respectively (see Fig. 2b). Cu'(A) and Cu'(B) indicate that these cations are in a unit cell adjacent to Cu(A) and Cu(B), respectively.

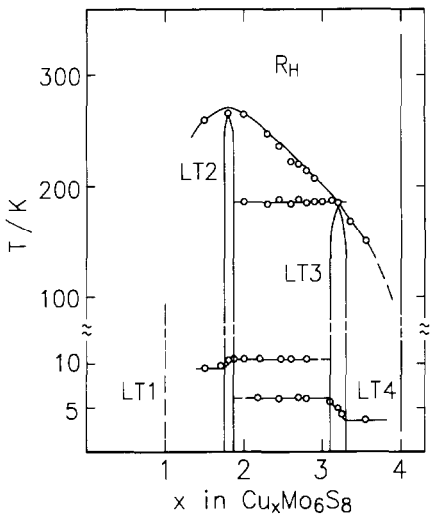

Fig. 19. The low temperature phase relations in the system $Cu_xMo_6S_{8-y}$, redrawn from ref. 14. Phase transformation temperatures and T_c are also plotted. R_H represents the rhombohedral high temperature phase (see Fig. 4).

that the A site (inner site) has an energy which is lower by 13 kJ mol^{-1} than the B site (outer site).

Many Chevrel phase sulfides undergo phase transformations near or below room temperature [39,40]. Flükiger et al. [14] have reported that the copper Chevrel phase $Cu_xMo_6S_{8-y}$ has four low temperature modifications in the range of $0 \leqslant x \leqslant 4$. Figure 19 shows the low temperature phase relations for $Cu_xMo_6S_{8-y}$. In the range $1.5 < x < 3.6$, the transition temperatures to the low temperature phase, determined by specific heat measurement, and the superconducting critical temperatures T_c (Flükiger et al. [41]) are also plotted. Three two-phase regions coexist with the region of four low temperature phases (LT1 through LT4 in Fig. 19). From X-ray diffraction results, it has been shown that LT2 (Fig. 19) crystallizes in a triclinic structure and LT4 in a rhombohedral form, while the structures for LT1 and LT3 are unknown [14]. The crystal structure of the low temperature modification (triclinic) of $Cu_{1.8}Mo_6S_8$ which corresponds to LT2 in Fig. 16 has been determined by Yvon et al. [8] and Baillif et al. [42]. The low temperature structure is illustrated in Fig. 20 together with the rhombohedral form for comparison. These are illustrated on the basis of the crystallographic data from ref. 8. The low temperature transformation is described as an ordering of the randomly occupied twelve metal sites in the rhombohedral structure onto two fixed lattice positions. Accordingly, this transformation would not occur when the compounds contain more than two cations per Mo_6S_8 formula unit.

Such a rhombohedral–triclinic transformation has also been observed for the following compounds: $Co_2Mo_6S_8$ (220 K) [39], $Fe_2Mo_6S_8$ (~ 400 K) [7],

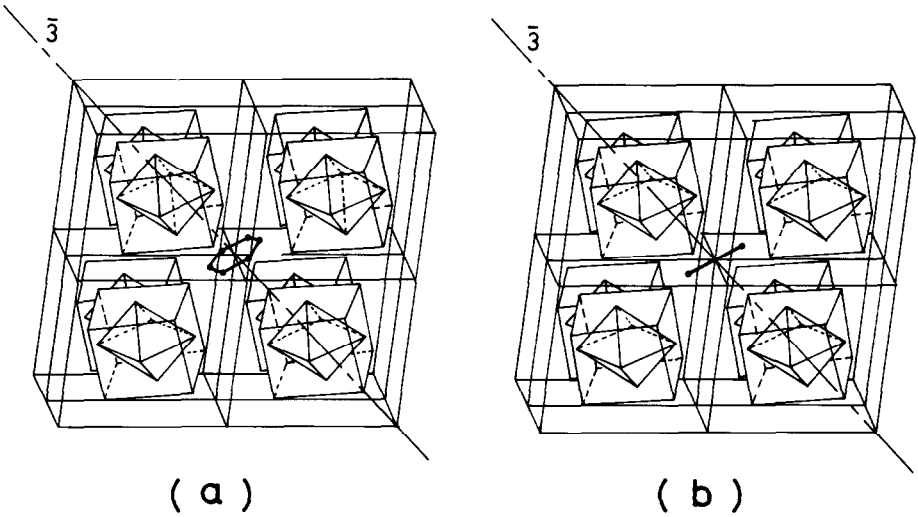

Fig. 20. Illustrations of the structures of (a) the rhombohedral high temperature form and (b) the triclinic low temperature modification of $Cu_{1.8}Mo_6S_8$, in the rhombohedral crystal lattice. Atomic positions are calculated from the data given in ref. 8. The outer sites of copper in the rhombohedral structure (a) are neglected for simplicity.

$ZnMo_5S_6$ (320 K) [40], $EuMo_6S_8$ (109 K) and $BaMo_6S_8$ (171 K) [43]; the transition temperatures are given in parentheses. The rhombohedral phases of $PbMo_6S_8$ [31], $AgMo_4S_5$ [39], $Ni_2Mo_6S_8$ [39] and Mo_6S_8 [40] are known to be stable down to 6 K.

Extensive measurements of specific heat near the superconducting critical temperatures T_c of the Chevrel phase sulfides have been carried out by many investigators. The specific heat measurement gives the most valuable information when the measurement is done over a sufficiently wide range of temperature. This temperature should be from about one-tenth of T_c to one-sixth of the Debye temperature [44]. Complete analysis of the data allows determination of the electronic specific heat coefficient and the (initial) Debye temperature $\Theta_D(T=0)$ including the formal variation $\Theta_D(T)$, a rough shape of the phonon spectrum $F(\omega)$, the thermodynamic critical field $H_c(T)$, the energy gap $\Delta(0)$ at $T=0$, etc. [44]. Also, this may give most of the parameters in the expression for T_c [45], such as the generalized moments of the phonon spectrum (ω_{log}, $\bar{\omega}_1$, $\bar{\omega}_2$ [45]), the electron phonon coupling parameter λ, the bare electron density state at the Fermi level $N_{bs}(E_F)$, etc [44].

The low temperature specific heat is measured by a heat pulse calorimeter [46], or a thermal relaxation type calorimeter [47,48].

The normal state specific heat C_n can be expressed as

$$C_n = \gamma T + \beta T^3 \tag{5}$$

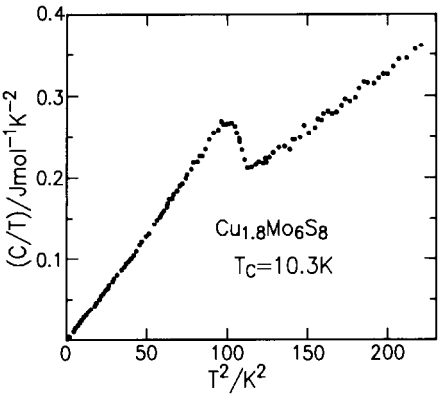

Fig. 21. Specific heat plotted as C/T vs. T^2, redrawn from ref. 50.

where γ and β represent coefficients of the electron and lattice contribution, respectively. Accordingly, C_n/T is usually plotted against T^2. At the T_c, owing to the formation of an energy gap, the density of states of the electron on the Fermi surface changes and a sudden increase of specific heat occurs (BCS theory [49]).

An example of the C/T vs. T_2 plot is shown in Fig. 21, which was measured for $Cu_{1.8}Mo_6S_8$ ($T_c = 10.3$ K) by Morohashi et al. [50].

However, detailed discussions on the variety of parameters derived from the specific heat measurement will not be made in this article, and we will simply refer to some papers in which heat capacity analyses of the Chevrel phase superconductors are described [50–52].

THERMAL OXIDATION OF THE CHEVREL PHASE SULFIDE

The stability of the Chevrel phase sulfides in air at elevated temperatures has been investigated by Takei et al. [53] and Taniguchi et al. [54] by means of thermogravimetry, differential thermal analysis and X-ray diffractometry. In Fig. 22, TG–DTA curves obtained by Taniguchi et al. and the DTA curve reported by Takei et al. (broken line) for $Cu_2Mo_6S_{8-y}$ are shown. For convenience, the DTA peaks are denoted as A1 to A4 (solid line, Taniguchi et al.) and B1 to B3 (broken line, Takei et al.). All the DTA peaks were exothermic.

Takei et al. used samples of about 50 mg and heating rates of 1–5 °C min^{-1}. Taniguchi et al. used samples of 5–20 mg and a heating rate was 10 °C min^{-1}. No change was observed below 200 °C. Both the peaks A1 and B1 were accompanied by a gradual weight gain. These peaks were thought to be due to oxygen pick-up by $Cu_2Mo_6S_{8-y}$. Takei et al. have concluded that CuO and $Cu_{-1}Mo_6S_8$ were formed at this stage instead of replacement of

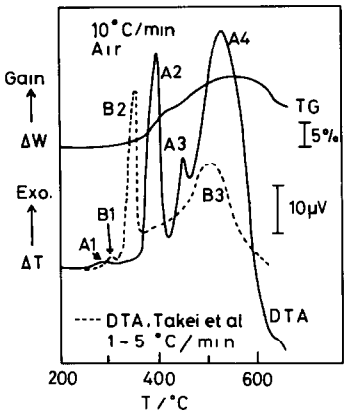

Fig. 22. TG–DTA curves for $Cu_2Mo_6S_{8-y}$, from refs. 50 and 51.

sulfur by oxygen; however, no X-ray peaks of CuO were observed. Taniguchi et al. have detected the formation of $Cu_{1.96}S$ at this stage. They have suggested that oxygen atoms substitute for sulfur, and $Cu_xMo_6S_{8-y}O_y$ ($x < 2$) and $Cu_{1.96}S$ were formed. In both cases, the copper contents x of the Chevrel phase were considerably lowered and an increase in the hexagonal c parameter was observed: $a_H = 9.612$ Å, $c_H = 10.247$ Å ($Cu_2Mo_6S_8$) → $a_H = 9.403$ Å, $c_H = 10.433$ Å ($Cu_{\sim 1}Mo_6S_8$) (Takei et al.); $a_H = 9.61$ Å, $c_H = 10.26$ Å ($Cu_2Mo_6S_{7.75}$) → $a_H = 9.42$ Å, $c_H = 10.35$ Å ($Cu_xMo_6S_{8-y}O_{1.99}$, $x < 2$) (Taniguchi et al.). It should be noted that these lattice parameters are approaching those of Mo_6S_8, i.e. $a_H = 9.200$ Å, $c_H = 10.880$ Å.

Although reaction temperatures were considerably different, very sharp DTA peaks (A2 and B2) were accompanied by rapid weight gains. These peaks were ascribed to the partial oxidation of the Chevrel phase to MoO_3. Accordingly, unreacted Chevrel phase still remains at this stage.

Taniguchi et al. have detected an independent small peak A3 before the broad and large peak A4. The X-ray diffraction analysis of the sample quenched at 466 °C (the temperature just before the A3 peak ended), clearly showed the formation of $CuSO_4$. Accordingly, the A3 peak would correspond to the reaction:

$$Cu_xMo_6S_{8-y}(\text{unreacted at A2}) + O_2 \rightarrow MoO_3 + CuSO_4 \quad (6)$$

The peaks A4 and B3 correspond to the final oxidation of the Chevrel phase to CuO, MoO_3 and/or to $CuMoO_4$ (at higher temperatures) according to the following equations:

$$2CuSO_4 \rightarrow CuO \cdot CuSO_4 + SO_3 \quad (7)$$

$$CuO \cdot CuSO_4 \rightarrow 2CuO + SO_3 \quad (8)$$

$$CuO + MoO_3 \rightarrow CuMoO_4 \quad (9)$$

REFERENCES

1 R. Chevrel, M. Sergent and J. Prigent, J. Solid State Chem., 3 (1971) 515.
2 B.T. Matthias, M. Marezio, E. Corenzwit, A.S. Cooper and H. Bars, Science, 175 (1972) 1465.
3 S. Foner, R. Odermatt, G. Bongi, H. Jones, R. Chevrel and M. Sergent, Phys. Lett. A, 49 (1974) 269.
4 W.R. Mckinnon and J.R. Dahn, Solid State Commun., 52 (1984) 245.
5 Y. Takeda, R. Kanno, M. Noda and O. Yamamoto, Mat. Res. Bull., 20 (1985) 71.
6 T. Uchida, K. Watanabe, M. Wakihara and M. Taniguchi, Chem. Lett., (1985) 1095.
7 K. Yvon, Current Topics, in E. Kaldis (Ed.), Materials Science, Vol. 3, North-Holland, 1979, p. 55.
8 K. Yvon, R. Baillif and R. Flükiger, Acta Crystallogr. B 35 (1979) 2859.
9 G. Krabbes and H. Oppermann, Cryst. Res. Tech., 16 (1971) 777.
10 K.Y. Cheung and B.C.H. Steele, Mater. Res. Bull., 15 (1980) 1717.
11 Ø. Fischer, Appl. Phys., 16 (1978) 1.
12 R. Srinivasan and V. Sankaranarayanan, Rev. Solid State Sci., 1 (1988) 463.
13 H. Wada, M. Onoda, H. Nozaki and I. Kawada, J. Less-Common Met., 113 (1985) 53.
14 R. Flükiger, R. Baillif and J. Muller, J. Less-Common Met., 72 (1980) 193.
15 S. Yamamoto, K. Matsui, M. Wakihara and M. Taniguchi, Mater. Res. Bull., 18 (1983) 1311.
16 J. Mizusaki, S.Y. Han, K. Fueki and K. Kitazawa, Solid State Ionics, 11 (1984) 293.
17 R. Chevrel, M. Sergent and J. Prigent, Mater. Res. Bull., 9 (1974) 1487.
18 J.M. Tarascon, J.V. Waszczak, G.W. Hull, F.J. Disalvo and L.D. Blitzer, Solid State Commun., 47 (1983) 973.
19 V.G. Krabbes and H. Oppermann, Z. Anorg. Allg. Chem., 481 (1981) 13.
20 J. Hauck, Mater. Res. Bull., 12 (1977) 1015.
21 S. Yamamoto, M. Wakihara and M. Taniguchi, Mater. Res. Bull., 20 (1985) 1493.
22 H. Yamasaki and Y. Kimura, Mater. Res. Bull., 21 (1986) 125.
23 R. Flükiger, R. Baillif and E. Walker, Mater. Res. Bull., 13 (1978) 743.
24 K. Yvon, R. Chevrel and M. Sergent, Acta Crystallogr. B, 36, 685 (1980).
25 H.A. Wagner and H.C. Freyhardt, J. Phys. Chem. Solids, 43 (1982) 177.
26 K. Sato, H. Hinode, M. Wakihara and M. Taniguchi, Mater. Res. Bull., 23 (1988) 993.
27 Y. Tanjo, T. Uchida and M. Wakihara, Denki Kagaku, 57 (1989) 553.
28 S. Yamaguchi, T. Uchida and M. Wakihara, J. Electrochem. Soc., in press.
29 P.J. Guillevic, O. Bars and D. Grandjean, Acta Crystallogr. B, 32 (1976) 1338.
30 M. Sergent, R. Chevrel, C. Rossel and Ø. Fischer, J. Less-Common Met., 58 (1978) 179.
31 M. Marezio, P.D. Dernier, J.P. Remeika, E. Corenzwit and B.T. Matthias, Mater. Res. Bull., 8 (1973) 657.
32 H. Yamasaki, Y. Yamaguchi and Y. Kimura, Mater. Res. Bull., 23 (1988) 23.
33 J. Hauck and M. Heiderich, Mater. Res. Bull., 17 (1982) 943.
34 I. Barin., O. Knacke and O. Kubaschewski, Thermochemical Properties of Inorganic Substances, Springer-Verlag, Berlin, 1973, p. 1977.
35 Y. Suzuki, T. Uchida, M. Wakihara and M. Taniguchi, Mater. Res. Bull., 16 (1981) 1085.
36 G.J. Dudley, K.Y. Cheung and B.C.H. Steele, J. Solid State Chem., 32 (1980) 259.
37 G.D. Dudley, K.Y. Cheung and B.C.H. Steele, J. Solid State Chem., 32 (1980) 269.
38 K. Yvon, A. Paoli, R. Flükiger and R. Chevrel, Acta Crystallogr. B, 33 (1977) 3066.
39 A.C. Lawson, Mater. Res. Bull., 7 (1972) 773.
40 A.C. Lawson and R.N. Shelton, Mater. Res. Bull., 12 (1977) 375.
41 R. Flükiger, A. Junod, R. Baillif, P. Spitzli, A. Treyvand, A. Paoli, H. Devantay and J. Muller, Solid State Commun., 23 (1977) 699.
42 R. Baillif, K. Yvon, R. Flükiger and J. Muller, J. Low Temp. Phys., 37 (1979) 231.

43 B. Lachal, R. Baillif, A. Junod and J. Muller, Solid State Commun., 45 (1983) 849.
44 A. Junod, T. Jarlborg and J. Muller, Phys. Rev. B, 27 (1983) 1569.
45 P.B. Allen and R.C. Dynes, Phys. Rev. B, 12 (1975) 905.
46 P. Spitzli, Arch. Sci., Geneve, 24 (1971) 145.
47 L.F. Mattheiss and C.Y. Fong., Phys. Rev. B, 115 (1977) 1760.
48 D.W. Bullett, Phys. Rev. Lett., 39 (1977) 664.
49 J. Bardeen, L.N. Cooper and J.R. Schrieffer, Phys. Rev., 108 (1957) 1175.
50 S. Morohashi, K. Noto, N. Kobayashi and Y. Muto, Physica B, 108 (1981) 929.
51 C. Hohfeld and B. Pietrass, J. Low Temp. Phys., 48 (1982) 503.
52 B. Lachal, A. Junod and J. Muller, J. Low Temp. Phys., 55 (1984) 195.
53 H. Takei, S. Hosoya and S. Tunekawa, Mater. Res. Bull., 21 (1986) 713.
54 M. Taniguchi, M. Wakihara and S.K. Basu, Solid State Ionics, 32/33 (1989) 273.